Lattice Energetics and Correlation-Driven Metal-Insulator Transitions: The Case of Ca$_2$RuO$_4$

Qiang Han[1] and Andrew Millis[1,2]

[1]*Department of Physics, Columbia University, New York, New York 10027, USA*
[2]*The Center for Computational Quantum Physics, The Flatiron Institute, New York, New York 10010, USA*

This Letter uses density functional, dynamical mean field, and Landau-theory methods to elucidate the interplay of electronic and structural energetics in the Mott metal-insulator transition. A Landau-theory free energy is presented that incorporates the electronic energetics, the coupling of the electronic state to local distortions and the coupling of local distortions to long-wavelength strains. The theory is applied to Ca$_2$RuO$_4$. The change in lattice energy across the metal-insulator transition is comparable to the change in electronic energy. Important consequences are a strongly first order transition, a sensitive dependence of the phase boundary on pressure and that the geometrical constraints on in-plane lattice parameter associated with epitaxial growth on a substrate typically change the lattice energetics enough to eliminate the metal-insulator transition entirely.

Many materials exhibit "Mott" metal-insulator transitions, primarily driven by electron-electron interactions [1] but also involving changes in atomic positions. In the rare earth titanates and vanadates, the distortion associated with the insulating phase is a GdFeO$_3$-type octahedral rotation [2,3], in the rare earth manganites, it is an approximately volume-preserving even-parity octahedral distortion [4–6]: in the perovskite nickelates, a two sublattice disproportionation of the mean Ni—O bond length [7–10] and in VO$_2$ a V—V dimerization [11]. In other materials including Ca$_2$RuO$_4$ [12] and V$_2$O$_3$ [13] the metal-insulator transition occurs simultaneously with a crystal symmetry-preserving change of atomic positions. The association of metal-insulator and structural transitions suggests the possibility of tuning electronic behavior by strain [14], epitaxial growth, or "nonlinear phononic" effects arising from intense terahertz radiation [15–17].

While electronic aspects of the Mott transition are becoming well understood, and energies, forces, and many-body structural relaxation are now available in beyond density functional frameworks such as the density functional plus dynamical mean field methodology [18–20], the interplay between the lattice and electronic energetics has yet to be fully unraveled. A physical basis for interpreting the calculations and the experiments remains to be defined and the magnitude of the lattice contribution to the energetics of the transition has yet to be determined. Here we argue that the key point is that the electronic transition couples directly to local atomic configurations such as octahedral rotations and transition metal-oxygen bond lengths, which in turn couple directly to externally controllable variables such as strain and pressure. The response of the material to these stresses defines a lattice stabilization energy, which can in fact be large enough to dominate the energetics of the transition.

To quantify these effects we write an electronic free energy $F^a(\delta\vec{Q})$ that depends on a state variable a labeling whether the material is in the metallic or insulating phase, and on atomic coordinates, labeled by a vector $\delta\vec{Q}$ expressing deviations of atomic positions from a reference configuration. Expanding in $\delta\vec{Q}$ we obtain

$$F^a(\delta\vec{Q}) = F_0^a + \vec{\mathcal{F}}^a \cdot \delta\vec{Q} + \frac{1}{2}\delta\vec{Q}^T \cdot \mathbf{K}^a \cdot \delta\vec{Q} + ... \quad (1)$$

The electronic state-dependent linear term $\vec{\mathcal{F}}^a$ specifies the force exerted by the electronic state on the atomic degrees of freedom (d.o.f.). Typically $\vec{\mathcal{F}}$ couples only to a subset of the lattice d.o.f., but this subset is coupled to other lattice coordinates by the quadratic restoring term $\mathbf{K}$. The ellipsis represents anharmonic terms that are not needed for the considerations of this Letter but may be important in other circumstances [4,21].

Minimizing the terms written in Eq. (1) gives $F = F_0^a - \frac{1}{2}\vec{\mathcal{F}}^{aT} \cdot \mathbf{K}^{-1} \cdot \vec{\mathcal{F}}^a$ defining the stabilization energy

$$F_{\text{stabil}}^a = -\frac{1}{2}\vec{\mathcal{F}}^{aT} \cdot \mathbf{K}^{-1} \cdot \vec{\mathcal{F}}^a, \quad (2)$$

so that if the lattice is free to relax, the transition between phases $a = 1, 2$ will occur when $F_0^1 + F_{\text{stabil}}^1 = F_0^2 + F_{\text{stabil}}^2$ corresponding to a shift in the transition point relative to a frozen lattice calculation and a lattice change across the transition $\delta\vec{Q}^1 - \delta\vec{Q}^2 = -\mathbf{K}^{-1}(\vec{\mathcal{F}}^1 - \vec{\mathcal{F}}^2)$.
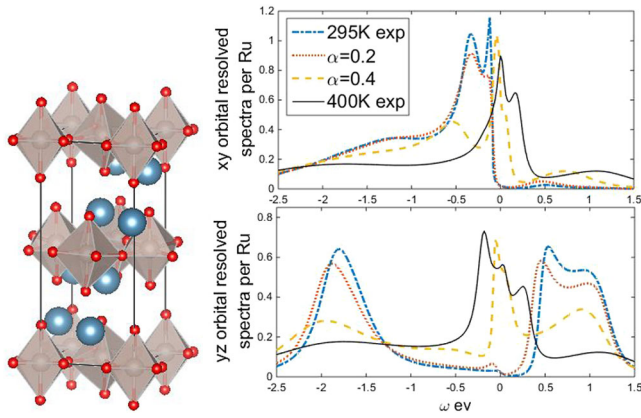
FIG. 1. Left panel: Representation of the unit cell of Ca_2RuO_4. Gray balls are ruthenium atoms, red balls oxygen atoms, and blue balls calcium atoms. Right panel: Orbitally resolved many-body densities of states for structures interpolating between experimental 295 and 400 K structures. Upper panel: xy orbital; lower panel: yz orbital (xz is very similar). $\alpha = 0$ is the 295 K structure; $\alpha = 1$ is the 400 K structure; $\alpha = 0.4$ is in the metallic phase but very close to the transition point; the $\alpha = 0.6, 0.8$ spectra are very similar to the 400 K spectra and are omitted for clarity.

We now apply these generic considerations to Ca_2RuO_4, which exhibits a correlation-driven paramagnetic metal to paramagnetic insulator transition as the temperature is decreased below a critical value about 350 K [12]. The transition is accompanied by a large amplitude, symmetry preserving lattice distortion [22,23]. Below about 140 K there is an onset of antiferromagnetic order [22,23], which is not relevant to our present considerations. Ca_2RuO_4 crystallizes in a *Pbca*-symmetry structure with four formula units in each crystallographic unit cell. The basic structural unit is the $Ru-O_6$ octahedron; these form corner-shared planes separated from adjacent $Ru-O_6$ planes by layers involving Ca atoms. The left panel of Fig. 1 shows one unit cell with four formula units. The *Pbca* structure is derived from the ideal tetragonal $n = 1$ Ruddlesden-Popper structure by rotations of the $Ru-O_6$ octahedrons about the apical $Ru-O(2)$ bonds, tilts of this axis with respect to the $Ru-O(1)$ plane, as well as an additional distortion that makes the two in-plane $Ru-O$ bond lengths slightly different. The apical $[Ru-O(2)]$ and the average over the two in-plane directions $[Ru-O(1)]$ $Ru-O$ bond lengths are the crucial variables in the electronic energetics. Their values across the metal-insulator transition are presented in Table I. The bond lengths continue to evolve as temperature is further lowered through the insulating phase [22,23]. The corner-shared structure implies that if the rotation angles remain fixed, the $Ru-O(1)$ bond lengths predict the average in-plane lattice parameters. Density functional calculations show that changes in the rotation angles are negligible for reasonable strains [24], so the in-plane $Ru-Ru$ and $Ru-O(1)$ distances are not independent variables. On the other hand, the c-axis stacking of the

TABLE I. Experimentally determined apical $[Ru-O(2)]$ and average in-plane $[Ru-O(1)]$ bond lengths and octahedral distortions [Eq. (3)] in Å at $T = 295$ [22] and 400 K [23], and occupancy (per spin per atom) of xy (n_{xy}), and average of yz, zx ($\bar{n}_{yz/zx}$) orbitals from DMFT calculation using the experimentally determined lattice structures at each temperature.

	RuO(2)	RuO(1)	δQ_0	δQ_3	n_{xy}	$\bar{n}_{yz/zx}$
400 K	2.042	1.95	0.0	0.0	0.671	0.665
295 K	1.995	1.99	0.0196	−0.069	0.982	0.508

Ruddlesden-Popper structure means that at fixed c-axis lattice constant, changes in the $Ru-O(2)$ bond length can be accommodated by a buckling of the $Ca-O$ planes.

We will be interested here in structures where the c-axis lattice parameter is relaxed for given values of the octahedral bond lengths. Thus the lattice d.o.f. in our theory are the average $Ru-O(1)$ and $Ru-O(2)$ lengths. We parametrize the $Ru-O$ bond lengths in terms of changes δx, δy, δz with respect to a reference state, which we take to be the 400 K metallic state, and we express these in terms of the octahedral coordinates

$$\delta Q_0 = \frac{1}{\sqrt{3}}(\delta z + \delta x + \delta y), \quad \delta Q_3 = \frac{1}{\sqrt{6}}(2\delta z - \delta x - \delta y), \quad (3)$$

which we assemble into the vector $\delta\vec{Q} = (\delta Q_3, \delta Q_0)$. **K** in Eq. (1) is defined from the dependence of energies on δQ_3 and δQ_0, with the c-axis lattice constant relaxed for each value of $\delta\vec{Q}$. We used density functional plus U (DFT + U) calculations and observed phonon frequencies (which give energetics of $Ru-O$ bond length changes without lattice relaxation) to estimate the entries of **K** (see Supplemental Material [24]), finding $K_{33} = 17.7$, $K_{03} = 7.6$, $K_{00} = 46.2 \text{ eV}/\text{Å}^2$ per formula unit. The observation [29–31] that the changes in optical phonon frequencies across the transition are about 2%, justifies the harmonic approximation and the independence of **K** on the electronic phase.

We now turn to the electronic d.o.f. The relevant frontier electronic states are t_{2g}-derived $Ru-4d$ oxygen $2p$ antibonding states which we refer to as Ru d states, following standard practice [32–36]. The t_{2g}-derived bands are well separated from the other bands, so we may focus our treatment of the correlation problem on them, treating the other bands as inert [34–36]. The tetragonal symmetry splits the t_{2g}-derived triplet into a singlet (d_{xy}) and a doublet (d_{xz} and d_{yz}). The octahedral rotations and other distortions (angles $\sim 10°$) provide small additional rearrangements of the level structure (in particular lifting the xz/yz degeneracy), but as long as the orbitals are defined with respect to the local octahedral symmetry axes, the deviations from the perfectly tetragonal structure do not significantly affect the on-site level splitting, basic energetics, or assignment of orbital character. Spin-orbit coupling ($\lambda_{SOC} \approx 0.1$ eV) is

important for lower T magnetic properties of the insulating state [31,37,38] but is not relevant to the physics we consider here since the spin-orbit energy scales are small compared to the orbital level splitting and electron interactions.

We have performed DFT and DFT + DMFT calculations (see Supplemental Material [39]). We find, in agreement with previous work [34], that a calculation at room temperature with the experimentally determined 400 K structure produces a moderately correlated metallic solution while using the 295 K structure produces a Mott insulator. The metallic state is characterized by an approximately equal occupancy of the three t_{2g} orbitals. The approximately equal orbital occupancy is not protected by any symmetry and is due to the strong electron-electron scattering. The insulating state is orbitally disproportionated, with an essentially fully filled xy band and half filled, much narrower, xz/yz bands with upper and lower Hubbard bands separated by a gap (Fig. 1 right panel with blue dashed lines). Calculated orbital occupancies are given in Table I.

The right-hand panels of Fig. 1 present the orbitally resolved densities of states obtained from DFT + DMFT calculations at room temperature, performed for a series of structures linearly interpolated between the $T = 295\ (\alpha = 0)$ and $T = 400\ \mathrm{K}\ (\alpha = 1)$ structures. As the interpolation parameter α changes from 1 to 0.4, the state remains metallic but the bands and occupancies (n_{xy}, n_{xz}, n_{yz}) change from $\approx (4/3, 4/3, 4/3)$ to $\approx (5/3, 7/6, 7/6)$. A first order MIT occurs as α is decreased below a critical value ≈ 0.4. Further changes of structure within the insulating phase ($\alpha = 0, 0.2$) do not affect the orbital occupancies but do lead to an approximately 0.1 eV shift upward of the xz/yz band relative to the xy band. We have also performed calculations in which one starts from the DFT + U relaxed insulating phase atomic positions with in-plane lattice constants fixed to 5.44 Å and the c-axis parameter is then gradually stretched. The results are very similar to the first group. Although the transition is first order we have not observed coexistence of metal and insulator phases at any of the lattice configurations we have studied.

Figure 2 plots the DFT + DMFT energy of the correlated bands (obtained as described in the Supplemental Material [39] for interpolated and c-axis stretched structures) against a linear combination of octahedral parameters [Eq. (3)].

$$E_{\mathrm{eff}} = E_{\mathrm{corr}} - \epsilon_{\mathrm{ave}} N_{\mathrm{tot}}$$
$$= E_0 - \mathcal{F}_3 (\delta Q_3 - \lambda_0 \delta Q_0 - \delta Q_c) \Theta (\delta Q_3 - \lambda_0 \delta Q_0 - \delta Q_c). \quad (4)$$

Here ϵ_{ave} is the orbitally averaged on-site energy from MLWF fits to the converged DFT band structures; $N_{\mathrm{tot}} = 4$, and $\epsilon_{\mathrm{ave}} N_{\mathrm{tot}}$ basically represents the insulating phase electron energy up to a constant. The particular linear combination with $\lambda_0 = 0.45$ is chosen so that the data from
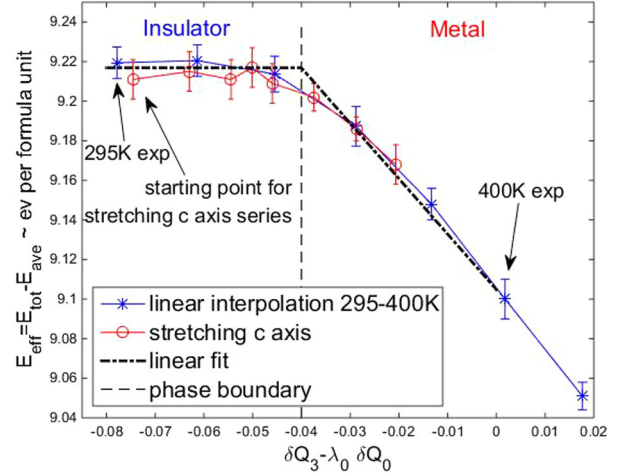

FIG. 2. Electronic energy of correlated bands $E_{\mathrm{eff}} = E_{\mathrm{corr}} - \epsilon_{\mathrm{ave}} N_{\mathrm{tot}}$ plotted against a linear combination of octahedral parameters with $\lambda_0 = 0.45$ and calculated using DFT + DMFT for two series of structures: the linearly interpolated structures between the experimentally observed metallic 400 K and insulating 295 K structures (solid points, blue) and a series obtained by starting from an relaxed insulating structure with $a = b = 5.44$ Å and stretching the c axis (open symbols, red). The bold dashed black line stands for the linear fit in Eq. (5) and the light dashed line shows the phase boundary. The error bars are statistical errors from the Monte Carlo solution of the DMFT equations.

the two different families of structures (which change the bandwidth and octahedral distortion in different proportions) collapses in both the insulating and metallic phases. The dependence on δQ_3 reflects the relation between the octahedral shape and the orbital splitting. The dependence on δQ_0 reflects the change in bandwidth. We emphasize that the insulating (metallic) state is only stable for $\delta Q_3 - 0.45 \delta Q_0 < (>) \delta Q_c \approx -0.04\ \overset{\circ}{A}$ (we expect δQ_c depends on U, J). Apart from some rounding in the immediate vicinity of the transition, the energy is a linear function of the relevant combination of the structural parameters, with a difference in slope between phases. The curvatures $\partial^2 E_{\mathrm{eff}} / \partial \delta Q^2$ in two phases are difficult to determine accurately from these calculations but are small enough compared with the $\mathbf{K}$ that any change in the $\mathbf{K}$ across the phase boundary is negligible (details are in the Supplemental Material [39]).

The choice of variables in Fig. 2 fixes the change in force across the transition as $\mathcal{F}_3 = \mathcal{F}_3^I - \mathcal{F}_3^M = 2.8$ and $\mathcal{F}_0 = \mathcal{F}_0^I - \mathcal{F}_0^M = -0.45(\mathcal{F}_3^I - \mathcal{F}_3^M) = -1.3\ \mathrm{eV}/\overset{\circ}{A}$. Within the assumptions made here, the dependence of the insulating phase energy on $\delta \vec{Q}$ is essentially independent of temperature. However, as temperature is further lowered through the paramagnetic insulating phase to the AFM phase transition, an approximately linear evolution of the Ru−O bonds lengths is observed [22,23], indicating an
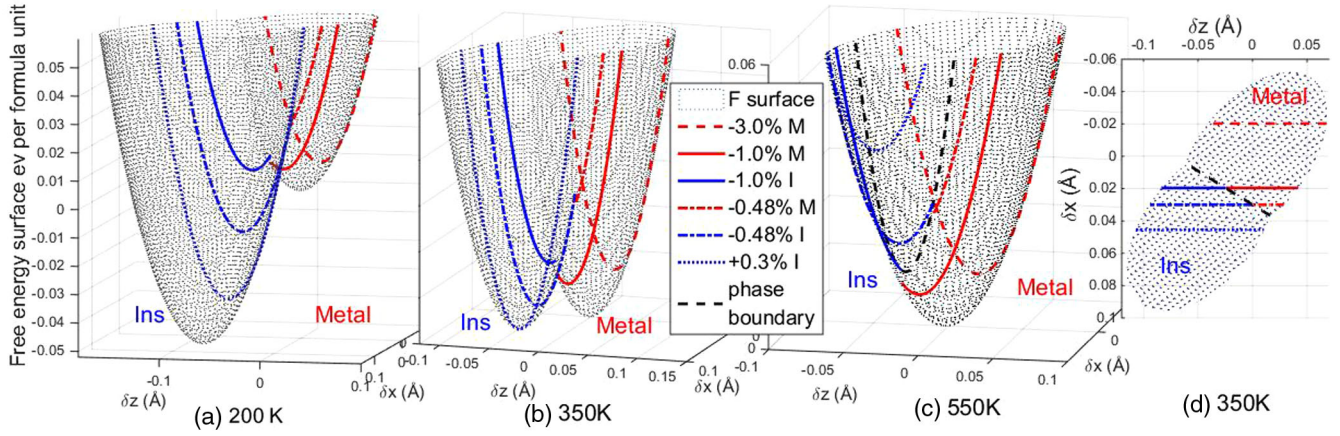
FIG. 3. Free energy surfaces computed for unconstrained bulk Ca_2RuO_4 at temperatures 200 (a), 350 (b), and 550 K (c). along with projection of the 350 K surface onto the $x - z$ plane (d). The black dashed line in panels (c) and (d) show the metal-insulator phase boundary. The solid and dashed lines show the structural trajectories which the system can explore for films grown under the epitaxial strain conditions given in the legends. The blue and red regions of the lines indicate insulating and metallic regions, respectively.

approximately T-linear dependence of the insulating-state force. Linearly extrapolating the Ru—O bond lengths measured in experiments [22,23] at 180, 295, and 350 K to 0 K yields results within 14% of our calculated values. We therefore believe that the single-site DMFT theory used here is a good representation of $T \to 0$ K energetics and that the temperature dependence is due to entropic terms arising from a combination of intersite effects missing in the single-site approximation used here, spin orbit effects which change the on-site multiplet structure and lattice contributions. We model these effect by a phenomenological linear term in $\vec{F}$, so

$$\vec{\mathcal{F}} = \begin{pmatrix} \mathcal{F}_3 \\ \mathcal{F}_0 \end{pmatrix} (1 - 0.0017 T[K]). \quad (5)$$

The consistency of the model can be verified via a computation of the pressure dependence of the transition. This is obtained by adding to Eq. (1) a term $+PdV = P\frac{1}{4}(ab\delta c + ac\delta b + bc\delta a) = P(\beta_3 \delta Q_3 + \beta_0 \delta Q_0)$ with $(\beta_3, \beta_0) = (-0.3281, -0.1861)$ eV/(GPa Å formula unit), so that applied pressure is in effect a linear term shifting the position and value of the energy minimum. We find $P_c = 3.6 - 0.011T$ (Gpa) which is comparable to $P_c^{\exp} \approx 2.3 - 0.006T$ (Gpa) fitted from published data [49]. More details are in the Supplemental Material [39].

In Fig. 3 we plot the free energy landscape at different temperatures in the plane of Ru—O bond length coordinates $\delta x = (1/\sqrt{3})\delta Q_0 - (1/\sqrt{6})\delta Q_3$ and $\delta z = (1/\sqrt{3})\delta Q_0 + (\sqrt{6}/3)\delta Q_3$, using force terms estimated in Eq. (5). We chose the metallic state at $T > T_{M-I}$ as the reference. At high temperature, there is no global minimum in the insulating phase. For $T \leq T_{M-I}$, an insulating energy minimum as in Eq. (2) appears and

becomes more stable. The stabilization energy defined in Eq. (2) is ≈ -0.048 eV/Ru at T_{M-I}.

We now turn to epitaxially grown films. While epitaxial films are strained with respect to bulk, strain is not the key issue. Rather, the tight association of the in-plane lattice parameter and the Ru—O(1) bond length means that epitaxy implies a constraint: instead of freely minimizing Eq. (1) over the full space of structural variables, the system can explore only a one-dimensional cut across the energy landscape, corresponding to a fixed Ru—O(1) bond length. The solid and dashed lines in Fig. 3 show the one-dimensional cuts which can be explored under different epitaxy conditions. Because the curves typically do not pass near the global minimum, the phase transition becomes much more expensive and in most cases is eliminated. Only in a small range of compressive strains around -1.0% (relative to 295 K structure) can a metal-insulator transition occur in a reasonable temperature range. For a larger compressive strain the system is always a metal while for a tensile or small compressive strain the material is always an insulator. This is consistent with recent experimental observations [50,51] that thin films of Ca_2RuO_4 grown epitaxially on $NdGaO_3$ ($+0.3\%$ strain) and NSAT (-0.48%) remain insulating up to 550 K while films grown on $NdAlO_3$ (-3.0%) remain metallic down to lowest temperature. Only films grown on $LaAlO_3$ (-1.6%) exhibit a transition to a weakly insulating phase at $T \approx 200$ K.

In summary, we demonstrated the importance of lattice energetics in the Mott metal-insulator transition, elucidating the crucial interplay between the local octahedral distortions and long wavelength strains, and the previously unappreciated role of epitaxial constraints. We focused on Ca_2RuO_4, which has two simplifying features: the metal and insulator have the same symmetry and octahedral rotations are of minor importance, so the order parameter

couples linearly to strains and the in-plane Ru—O bond lengths determine the Ru—Ru spacing. Performing a complete DFT + DMFT structural relaxation study and providing a less phenomenological treatment of the electronic and, especially, lattice entropies are also important directions for future research. Most importantly, a generalization of the theory to cases where octahedral rotation is important (perovskite titanates and vanadates) or the insulating phase breaks a translation symmetry (manganites and nickelates) so that strain couples via nonlinear terms in the elastic theory, is urgently needed.

[1] M. Imada, A. Fujimori, and Y. Tokura, Rev. Mod. Phys. **70,** 1039 (1998).

[2] M. Cwik, T. Lorenz, J. Baier, R. Müller, G. André, F. Bourée, F. Lichtenberg, A. Freimuth, R. Schmitz, E. Müller-Hartmann, and M. Braden, Phys. Rev. B **68,** 060401 (2003).

[3] E. Pavarini, S. Biermann, A. Poteryaev, A. I. Lichtenstein, A. Georges, and O. K. Andersen, Phys. Rev. Lett. **92,** 176403 (2004).

[4] A. J. Millis, P. B. Littlewood, and B. I. Shraiman, Phys. Rev. Lett. **74,** 5144 (1995).

[5] A.-M. Haghiri-Gosnet and J. P. Renard, J. Phys. D **36,** R127 (2003).

[6] Y. Tokura, Rep. Prog. Phys. **69,** 797 (2006).

[7] J. B. Torrance, P. Lacorre, A. I. Nazzal, E. J. Ansaldo, and C. Niedermayer, Phys. Rev. B **45,** 8209 (1992).

[8] J. A. Alonso, J. L. García-Muñoz, M. T. Fernández-Díaz, M. A. G. Aranda, M. J. Martínez-Lope, and M. T. Casais, Phys. Rev. Lett. **82,** 3871 (1999).

[9] M. T. Fernández-Díaz, J. A. Alonso, M. J. Martínez-Lope, M. T. Casais, J. L. García-Muñoz, and M. A. G. Aranda, Physica (Amsterdam) **276B–278B,** 218 (2000).

[10] M. Medarde, C. Dallera, M. Grioni, B. Delley, F. Vernay, J. Mesot, M. Sikora, J. A. Alonso, and M. J. Martínez-Lope, Phys. Rev. B **80,** 245105 (2009).

[11] F. J. Morin, Phys. Rev. Lett. **3,** 34 (1959).

[12] S. Nakatsuji, S. ichi Ikeda, and Y. Maeno, J. Phys. Soc. Jpn. **66,** 1868 (1997).

[13] D. B. McWhan, T. M. Rice, and J. P. Remeika, Phys. Rev. Lett. **23,** 1384 (1969).

[14] T. Kikuzuki and M. Lippmaa, Appl. Phys. Lett. **96,** 132107 (2010).

[15] M. Rini, R. Tobey, N. Dean, J. Itatani, Y. Tomioka, Y. Tokura, R. W Schoenlein, and A. Cavalleri, Nature (London) **449,** 72 (2007).

[16] H. Ehrke, R. I. Tobey, S. Wall, S. A. Cavill, M. Först, V. Khanna, T. Garl, N. Stojanovic, D. Prabhakaran, A. T. Boothroyd, M. Gensch, A. Mirone, P. Reutler, A. Revcolevschi, S. S. Dhesi, and A. Cavalleri, Phys. Rev. Lett. **106,** 217401 (2011).

[17] H. Ichikawa, S. Nozawa, T. Sato, A. Tomita, K. Ichiyanagi, M. Chollet, L. Guérin, N. Dean, A. Cavalleri, S-i. Adachi, T-h. Arima, H. Sawa, Y. Ogimoto, M. Nakamura, R. Tamaki, K. Miyano, and S-y. Koshihara, Nat. Mater. **10,** 101 (2011).

[18] H. Park, A. J. Millis, and C. A. Marianetti, Phys. Rev. B **89,** 245133 (2014).

[19] I. Leonov, V. I. Anisimov, and D. Vollhardt, Phys. Rev. Lett. **112,** 146401 (2014).

[20] K. Haule and G. L. Pascut, Phys. Rev. B **94,** 195146 (2016).

[21] J. Kanamori, J. Appl. Phys. **31,** S14 (1960).

[22] M. Braden, G. André, S. Nakatsuji, and Y. Maeno, Phys. Rev. B **58,** 847 (1998).

[23] O. Friedt, M. Braden, G. André, P. Adelmann, S. Nakatsuji, and Y. Maeno, Phys. Rev. B **63,** 174432 (2001).

[24] See Supplemental Material at http://link.aps.org/supplemental/10.1103/PhysRevLett.121.067601. See Sec. I for details of DFT + U calculation and estimation of stiffness matrix **K**, which includes Refs. [25–28] not cited in the main text.

[25] G. Kresse and J. Hafner, Phys. Rev. B **47,** 558 (1993).

[26] G. Kresse and J. Furthmüller, Comput. Mater. Sci. **6,** 15 (1996).

[27] G. Kresse and J. Furthmüller, Phys. Rev. B **54,** 11169 (1996).

[28] G. Kresse and D. Joubert, Phys. Rev. B **59,** 1758 (1999).

[29] H. Rho, S. L. Cooper, S. Nakatsuji, H. Fukazawa, and Y. Maeno, Phys. Rev. B **71,** 245121 (2005).

[30] J. H. Jung, Z. Fang, J. P. He, Y. Kaneko, Y. Okimoto, and Y. Tokura, Phys. Rev. Lett. **91,** 056403 (2003).

[31] S.-M. Souliou, J. Chaloupka, G. Khaliullin, G. Ryu, A. Jain, B. J. Kim, M. Le Tacon, and B. Keimer, Phys. Rev. Lett. **119,** 067201 (2017).

[32] P. B. Allen, H. Berger, O. Chauvet, L. Forro, T. Jarlborg, A. Junod, B. Revaz, and G. Santi, Phys. Rev. B **53,** 4393 (1996).

[33] J. S. Ahn, J. Bak, H. S. Choi, T. W. Noh, J. E. Han, Y. Bang, J. H. Cho, and Q. X. Jia, Phys. Rev. Lett. **82,** 5321 (1999).

[34] E. Gorelov, M. Karolak, T. O. Wehling, F. Lechermann, A. I. Lichtenstein, and E. Pavarini, Phys. Rev. Lett. **104,** 226401 (2010).

[35] H. T. Dang, J. Mravlje, A. Georges, and A. J. Millis, Phys. Rev. B **91,** 195149 (2015).

[36] Q. Han, H. T. Dang, and A. J. Millis, Phys. Rev. B **93,** 155103 (2016).

[37] D. Sutter, C. Fatuzzo, S. Moser, M. Kim, R. Fittipaldi, A. Vecchione, V. Granata, Y. Sassa, F. Cossalter, G. Gatti, M. Grioni, H. Ronnow, N. Plumb, C. Matt, M. Shi, M. Hoesch, T. Kim, T. Chang, H. Jeng, C. Jozwiak et al., Nat. Commun. **8,** 15176 (2017).

[38] M. Kim, J. Mravlje, M. Ferrero, O. Parcollet, and A. Georges, Phys. Rev. Lett. **120,** 126401 (2018).

[39] See Supplemental Material at http://link.aps.org/supplemental/10.1103/PhysRevLett.121.067601. See Sec. II for details of DFT, DFT + DMFT calculation, and

calculations of electronic energetic and force terms $\vec{\mathcal{F}}$, which includes Refs. [40–48] not cited in the main text.

[40] H. T. Dang and A. J. Millis, Phys. Rev. B **87,** 155127 (2013).

[41] N. Marzari and D. Vanderbilt, Phys. Rev. B **56,** 12847 (1997).

[42] I. Souza, N. Marzari, and D. Vanderbilt, Phys. Rev. B **65,** 035109 (2001).

[43] J. Kanamori, Prog. Theor. Phys. **30,** 275 (1963).

[44] O. Parcollet, M. Ferrero, T. Ayral, H. Hafermann, I. Krivenko, L. Messio, and P. Seth, Comput. Phys. Commun. **196,** 398 (2015).

[45] P. Seth, I. Krivenko, M. Ferrero, and O. Parcollet, Comput. Phys. Commun. **200,** 274 (2016).

[46] J. Chen, A. J. Millis, and C. A. Marianetti, Phys. Rev. B **91,** 241111 (2015).

[47] T. Pruschke, D. L. Cox, and M. Jarrell, Phys. Rev. B **47,** 3553 (1993).

[48] P. Steffens, O. Friedt, P. Alireza, W. G. Marshall, W. Schmidt, F. Nakamura, S. Nakatsuji, Y. Maeno, R. Lengsdorf, M. M. Abd-Elmeguid, and M. Braden, Phys. Rev. B **72,** 094104 (2005).

[49] F. Nakamura, J. Phys. Soc. Jpn. **76,** 96 (2007).

[50] H. Nair, J. Ruf, Y. Liu, N. Shukla, B. Grisafe, C. S. Chang, Q. Han, A. Millis, D. A. Muller, S. Datta, K. Shen, and D. G. Schlom, http://ceramics.org/wp-content/uploads/2017/01/EMA2017_WebFinal-2.pdf.

[51] C. Dietl, S. K. Sinha, G. Christiani, Y. Khaydukov, T. Keller, D. Putzky, S. Ibrahimkutty, P. Wochner, G. Logvenov, P. A. van Aken, B. J. Kim, and B. Keimer, Appl. Phys. Lett. **112,** 031902 (2018).